Incommensurate spin order in the metallic perovskite $MnVO_3$

Mikael Markkula,[1] Angel M. Arevalo-Lopez,[1] Anna Kusmartseva,[1] Jennifer A. Rodgers,[1] Clemens Ritter,[2] Hua Wu,[3,4] and J. Paul Attfield[1,*]

[1] *Centre for Science at Extreme Conditions and School of Chemistry, University of Edinburgh, Mayfield Road, Edinburgh EH9 3JZ, United Kingdom*

[2] *Institut Laue-Langevin, BP 156, F-38042 Grenoble Cedex 9, France*

[3] *II. Physikalisches Institut, Universität zu Köln, D-50937 Köln, Germany*

[4] *Department of Physics, Fudan University, Shanghai, China*

(Received 22 August 2011; published 28 September 2011)

Incommensurate Mn spin order has been discovered in the perovskite $MnVO_3$ containing localized $3d^5$ Mn^{2+} and itinerant $3d^1$ V^{4+} states. This phase has a distorted *Pnma* crystal structure ($a = 5.2741(6)$ Å, $b = 7.4100(11)$ Å, and $c = 5.1184(8)$ Å at 300 K) and is metallic at temperatures of 2–300 K and at pressures of up to 67 kbar. Neutron scattering reveals a (0.29 0 0) magnetic vector below the 46 K spin ordering transition, and both helical and spin density wave orderings are consistent with the diffraction intensities. Electronic structure calculations show large exchange splittings of the Mn and V 3d bands, and (k_x 0 0) crossings of the Fermi energy by spin up and down V 3d bands may give rise to Ruderman-Kittel-Kasuya-Yosida coupling of Mn moments, in addition to their superexchange interactions.

DOI: 10.1103/PhysRevB.84.094450 PACS number(s): 75.30.Et, 75.47.Lx, 75.25.−j, 72.80.Ga

I. INTRODUCTION

Many notable properties (e.g., superconductivity, magnetism, and multiferroicity) emerge from d-electron correlations in ABO_3 perovskite oxides. Perovskites of orbitally degenerate transition metal cations synthesized under high pressure and temperature are often far from equilibrium when recovered to ambient conditions, and this thermodynamic instability may be expressed through unusual electronic phenomena. For example, $SrCrO_3$ undergoes an orbitally driven electronic phase separation at low temperatures,[1–3] and $PbRuO_3$ shows an unusual symmetry reversing transition associated with orbital order[4,5] that is not observed in other $ARuO_3$ ruthenates.

AVO_3 perovskites of $3d^1$ V^{4+} have been synthesized at ambient pressure for A = Ca and Sr and at high pressures (4–7 GPa) for A = Cd, Pb, and Mn. The ambient pressure perovskites $CaVO_3$ and $SrVO_3$ are metallic,[6,7] and $CaVO_3$ shows a well-defined Fermi surface arising from itinerant $3d^1$ V^{4+} states.[8] $CdVO_3$ is also metallic and Pauli paramagnetic[9]; however, $PbVO_3$ is an antiferromagnetic, ferroelectric insulator with coupled, off-center distortions of the Pb^{2+} and V^{4+} ions.[10,11] Thin films of $PbVO_3$ have been grown at ambient pressures, and piezoelectric and nonlinear optical activity were reported.[12,13] The high-pressure perovskite $MnVO_3$ was reported to be a Curie-Weiss paramagnet with a relatively low electric resistivity.[14] The physical properties of this phase are of interest, because Mn^{2+} is smaller than the other A cations, which is expected to reduce the width of the V d-band and increase electron–electron correlation, and the $S = 5/2$ $3d^5$ Mn^{2+} moments may couple to the $3d^1$ V^{4+} states, leading to complex magnetic order. We describe here an investigation of the lattice, electronic, and magnetic properties of this unusual "A-site manganite" using polycrystalline high-pressure samples. This demonstrates that the Mn^{2+} and V^{4+} electron states are localized and itinerant, respectively, and an incommensurate order of the Mn^{2+} spins at low temperatures may evidence both frustrated superexchange interactions and Ruderman-Kittel-Kasuya-Yosida (RKKY) coupling through the V^{4+} band.

II. SAMPLE PREPARATION

Small ceramic samples of $MnVO_3$ were synthesized via the same multianvil Walker press method used to prepare the high-pressure perovskites $SrCrO_3$ and $PbRuO_3$.[3,4] A $Mn_2V_2O_7$ precursor, synthesized from a mixture of MnO and V_2O_5 at 750 °C, was reduced to $MnVO_3$ perovskite at high pressure and temperature. The optimum conditions were found to be heating at 1100 °C under 8 GPa of pressure for 30 min, followed by a quench to ambient temperature and depressurization. Powder x-ray diffraction confirmed that $MnVO_3$ adopts an orthorhombic *Pnma* perovskite structure. Six high-pressure products were combined to give a 77-mg $MnVO_3$ sample for synchrotron x-ray and neutron powder diffraction measurements. High-resolution synchrotron data from the ID31 beamline at the European Synchrotron Radiation Facility (ESRF) showed that $MnVO_3$ adopts an orthorhombic *Pnma* perovskite superstructure without further lattice distortions, and no structural transitions or anomalies were observed between 4 and 300 K. The refined structural parameters were in agreement with those from neutron analysis, as described later.

III. MAGNETIZATION AND CONDUCTIVITY MEASUREMENTS

Magnetization measurements for $MnVO_3$ in a 0.1-T field are similar to those in the original report[14] and show an ordering transition near $T_N = 50$ K and Curie-Weiss paramagnetism at higher temperatures. A fit to inverse susceptibility data between 120 and 200 K gives a paramagnetic moment of 5.80 μ_B, close to the theoretical value of 5.91 μ_B for localized $S = 5/2$ Mn^{2+}, and a Weiss temperature of $\theta = -154$ K, showing that antiferromagnetic spin–spin interactions are dominant and partly frustrated ($|\theta|/T_N \approx 3$).

 ©2011 American Physical Society

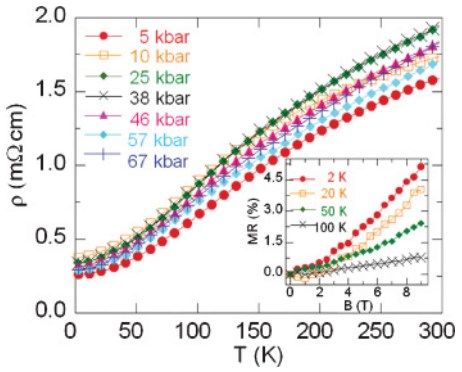

FIG. 1. (Color online) Resistivity of a ∼150-μm $MnVO_3$ pellet fragment at pressures of 5–67 kbar. The inset shows the field dependence of magnetoresistance at 2–100 K under 5 kbar of pressure.

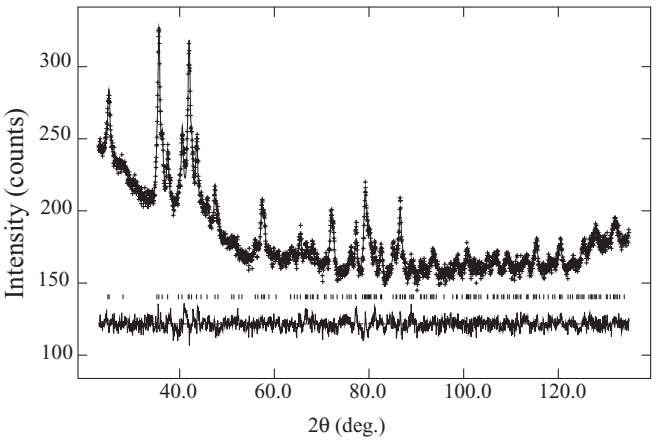

FIG. 2. Fit to the 300-K D2B neutron diffraction profile of $MnVO_3$, from which the refined parameters shown in Table I were derived.

Four-probe resistivity measurements from sintered ceramic $MnVO_3$ bars at ambient pressure gave inconsistent results that probably reflect poor interparticle connections or contact or grain boundary resistances. However, applying pressures of a few kilobars within a diamond anvil cell revealed a reproducible metallic behavior with a residual resistivity of $\rho_0 \approx 300$ $\mu\Omega$ cm (Fig. 1). The temperature dependence of the resistivity is described well by a conventional Fermi liquid $\rho = \rho_0 + CT^2$ variation at low temperatures, and enhanced phonon or electronic correlations are not apparent. This behavior does not change significantly up to 67 kbar of pressure, and no electronic transitions are evident down to 2 K in this pressure range, showing that the metallic state is robust and no proximity to a metal-insulator phase boundary is manifest. A small positive magnetoresistance is observed in applied fields up to 9 T, and the magnitude increases on cooling (Fig. 1 inset). This is characteristic of the normal (Lorentz force) magnetoresistance of a metal, and the absence of resistance and magnetoresistance discontinuities at the 50-K magnetic transition shows that the conductivity is not strongly coupled to the spin order, in contrast to metallic *B*-site manganites, e.g., $La_{1-x}Ca_xMnO_3$, which show colossal negative magnetoresistances.

IV. NEUTRON DIFFRACTION STUDIES

A high-resolution neutron diffraction profile (Fig. 2) collected at a wavelength of 1.594 Å from instrument D2B at the Institut Laue-Langevin (ILL) was used to refine the crystal structure of $MnVO_3$. Refinement results are shown in Table I, and derived bond distances and angles are in Table II. The structure adopts a highly distorted *Pnma* arrangement in which the 12 *A*-O distances, which are equivalent in a cubic perovskite, are split into sets of four short (2.2 Å), four medium (2.4–2.6 Å), and four long (3.1–3.4 Å) Mn-O bonds. The VO_6 octahedra are tetragonally compressed with two short (1.88 Å) and four long (1.95–1.98 Å) V-O distances, in contrast to $CaVO_3$ and $SrVO_3$, where the octahedra are nearly regular.[6,7] This would be consistent with an orbital ordering of localized $3d^1$ V^{4+} states if $MnVO_3$ were insulating, but because this material is metallic it more likely reflects the intrinsic distortions caused by the mismatch between the Mn-O and the V-O distances *D*. The ABO_3 perovskite tolerance factor $t = D(A-O)/\sqrt{2}D(B-O)$ has an ideal value of $t = 1$ for a cubic structure, but orthorhombic $MnVO_3$ has $t = 0.89$.

Further neutron data were collected between 1.7 and 60 K in 1-K steps from the ILL's instrument D20 at a wavelength of 2.418 Å to explore the spin order in $MnVO_3$. Magnetic diffraction peaks appear below 46 K [Fig. 3(a)] and are all indexed by propagation vector $k = (k_x\ 0\ 0)$. The magnitude of the orthorhombic structural distortion is sufficient to enable alternative vectors, e.g., $(0\ k_y\ 0)$ or $(0\ 0\ k_z)$, to be excluded because they do not match the peak positions. k_x varies slightly with temperature, from $k_x = 0.2903(4)$ at 1.7 K to $k_x = 0.3015(9)$ at 43 K. The incommensurate magnetic structure was refined using representation analysis within the FULLPROF software package.[15] The $(k_x\ 0\ 0)$ order of *A*-site spins within a *Pnma* perovskite has previously been analyzed

TABLE I. Refined *x*-, *y* -, and *z*-coordinates and isotropic atomic displacement (U_{iso}) factors in space group *Pnma* for $MnVO_3$ at 300 K. Cell parameters were $a = 5.2741(6)$, $b = 7.4100(11)$, and $c = 5.1184(8)$ Å; the fitting residuals were $\chi^2 = 1.65$; and the weighted profile residual was $R_{wp} = 0.021$. Mn and V were constrained to have the same U_{iso}.

Atom	*x*	*y*	*z*	U_{iso} (Å^2)
Mn	0.0630(21)	0.25	0.4853(22)	0.017(3)
V	0	0	0	0.017
O1	0.4551(12)	0.25	0.6074(12)	0.009(2)
O2	0.2983(9)	0.0582(6)	0.1842(8)	0.010(1)

TABLE II. Interatomic distances and angles for the perovskite $MnVO_3$ at 300 K.

	Distance (Å)		Distance (Å)
Mn-O1	3.266(11)	V-O1 (×2)	1.947(2)
Mn-O1	2.161(11)	V-O2 (×2)	1.884(4)
Mn-O1	3.086(11)	V-O2 (×2)	1.982(4)
Mn-O1	2.161(12)		
Mn-O2 (×2)	2.436(9)		Angle (°)
Mn-O2 (×2)	2.173(9)	V-O1-V	144.2(3)
Mn-O2 (×2)	2.605(6)	V-O2-V	143.7(3)
Mn-O2 (×2)	3.422(10)		

for $TbMnO_3$,[16–18] and below we use the corepresentation analysis from Table IV of Ref. 17, where the application of an antiunitary operator for inversion of the propagation vector gives a fuller symmetry description than do conventional irreducible representations.

The magnetic neutron diffraction intensities of $MnVO_3$ are not described well by a single spin corepresentation, but a good fit was obtained using a combination of $D_3(m_z)$ and $D_4(m_y)$ vectors of equal magnitude 3.45(14) μ_B at 1.7 K. (Independent refinement gave insignificantly different values of 3.45(18) and 3.46(16) μ_B for the respective vectors, without improvement to the profile fit.) Each describes a sine-wave spin component, but the fits are inherently insensitive to the phase difference between the two vectors, leading to two descriptions of the spin structure [Figs. 3(b) and 3(c)]. An out-of-phase combination (e.g., $D_3 + iD_4$) generates a helical spin structure with a constant ordered Mn moment of 3.5(1) μ_B at 1.7 K, but an in-phase sum (e.g., $D_3 + D_4$) describes a sinusoidal spin density wave (SDW) of collinear moments with an amplitude of $\sqrt{2} \times 3.5 = 4.9(2)\,\mu_B$, corresponding to the ideal moment of $5\,\mu_B$ for $S = 5/2$ Mn^{2+}. Hence, both spin ordering possibilities are physically realistic. The equal magnitudes of the m_y and m_z components suggest a helical order but do not exclude an SDW in the (011) plane. The ordered moment has the theoretical value for an SDW of Mn^{2+} spins, but a reduced value of 3.5(1) μ_B is plausible in a helimagnet as spin order is partly frustrated. The fit of a critical law $m(T) = m(0)[1 - (T/T_N)]^\beta$ to the magnetic moment m in the temperature range $T_N/2 < T < T_N$ (Fig. 4) gives $T_N = 46.3(6)$ K and $\beta = 0.32(3)$. The critical exponent agrees well with the theoretical value of 0.34 for a three-dimensional xy-magnet, which is appropriate to $MnVO_3$ because spins are constrained to lie in the yz-plane in both ordering descriptions. No B-site spin order was observed, but the possibility of a small ordered component

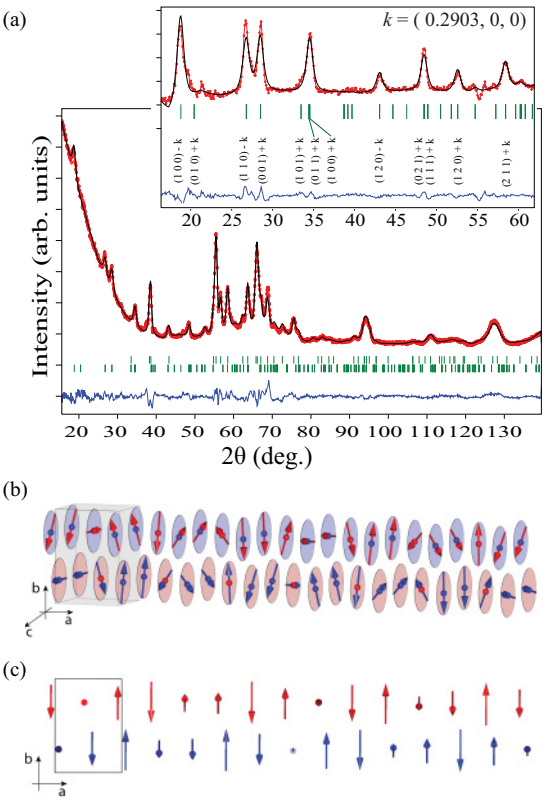

FIG. 3. (Color online) Incommensurate magnetic order in $MnVO_3$. (a) Fit of the nuclear and magnetic structures (upper and lower tick marks) to the D20 neutron powder diffraction profile of $MnVO_3$ at 1.7 K. The inset difference between 1.7- and 60-K patterns shows magnetic satellite reflections indexed by the propagation vector $k = (0.2903\ 0\ 0)$. Two ordering models give equivalent fits to the neutron data: (b) a helimagnetic spiral, in which all Mn moments have an equal magnitude of 3.5 μ_B, and (c) a SDW of collinear moments parallel to the [011] plane, with an amplitude of 4.9 μ_B.

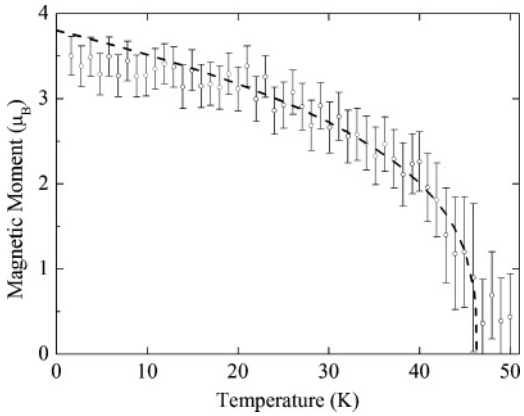

FIG. 4. Variation of the ordered Mn moment [in the helical model of Fig. 3(b)] with temperature for $MnVO_3$, showing the critical law fit described in the text.

at the V sites is not excluded by the present powder neutron diffraction measurements.

Helical spin structures are of interest because they can break inversion symmetry and generate coupled electrical and magnetic polarizations (multiferroicity), e.g., in the *B*-site manganite $TbMnO_3$.[15–17] However, the symmetry constraints for electrical polarization in Table II of Ref. 17 show that the $D_3 + iD_4$ corepresentation of $MnVO_3$ belongs to the nonpolar point group 222, so no ferroelectric polarization is predicted from the helical model in Fig. 3(b). The observed metallic conductivity of $MnVO_3$ precludes measurement of electrical polarization.

V. BAND STRUCTURE CALCULATIONS

Electronic structure calculations within the local density approximation (LDA) were performed for the 300-K neutron model of $MnVO_3$ using the full-potential augmented plane-wave plus local-orbital method.[19] The muffin-tin sphere radii were 2.5, 2.0, and 1.5 Bohr for Mn, V, and O atoms, respectively. A cutoff energy of 12 Ryd was set for the plane-wave expansion of interstitial wave functions, and an $8 \times 6 \times 8$ $\boldsymbol{k}$-mesh was used for integration over the first Brillouin zone.

The calculated band structure (Fig. 5) shows a large exchange splitting of the Mn 3d bands, giving rise to local Mn^{2+} $S = 5/2$ spins, and the V 3d band has an apparent exchange splitting of ~1.0 eV. The $3d^1$ V^{4+} band is almost completely spin polarized with an antiferromagnetic Mn-V exchange interaction, which was calculated to be more stable than the ferromagnetic Mn-V state by 20 meV/formula unit (f.u.). Thus, $MnVO_3$ is predicted to be a magnetic metal with localized majority Mn^{2+} $S = 5/2$ spins and an itinerant minority spin V^{4+} $3d^1$ band. However, an alternative magnetic ground state with a ferromagnetic Mn order and an A-type antiferromagnetic V order was found to have the same energy within 1 meV/f.u., suggesting that competing interactions are likely to be present in $MnVO_3$.

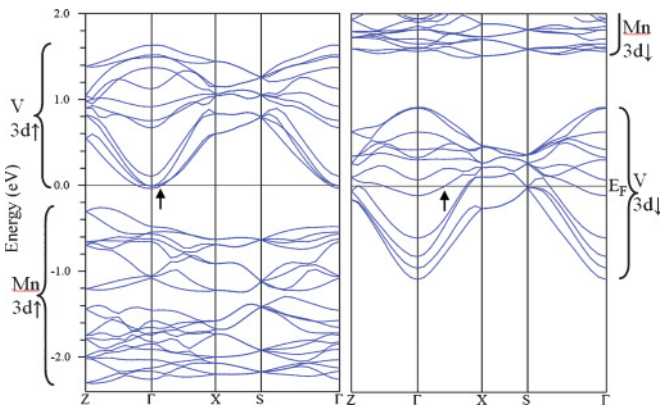

FIG. 5. (Color online) Spin up and down Mn 3d and V 3d(t_{2g}) band dispersions (20 and 12 bands, respectively, for the *Pnma* cell containing four $MnVO_3$ units) from the LDA computed band structure. V 3d(t_{2g}) bands crossing the Fermi energy at (k_x 0 0) are marked by arrows on the Γ-*X* sections.

VI. DISCUSSION

The preceding results show that $MnVO_3$ is a metallic oxide in which the V 3d band electrons remain itinerant down to at least 2 K over a wide pressure range and the Mn^{2+} spins are localized and undergo an incommensurate antiferromagnetic order below 46 K. The coupling mechanism between Mn spins is of particular interest because both insulating superexchange and itinerant electron RKKY scenarios are plausible. In an ideal cubic $MnBO_3$ perovskite, each Mn cation is connected to 12 next-nearest neighbors through linear Mn-O-Mn bridges that mediate the dominant antiferromagnetic superexchange interactions. These interactions are frustrated, but the *Pnma* distortion breaks the equivalence of many of the connections so that helical order can arise for a particular balance of superexchange strengths. However, the O 2s and 2p states that mediate Mn-O-Mn superexchange are also strongly hybridized with the V 3d(t_{2g}) band, providing a mechanism for coupling the localized Mn $S = 5/2$ spins to the V conduction electrons.

The (k_x 0 0) spin modulation results in a net magnetization at each V and O site as the surrounding Mn moments do not cancel to zero, although V atoms lie at the center of inversion symmetry in the *Pnma* structure, Hence, an RKKY interaction in which the Mn spins are indirectly coupled through their interaction with the V 3d conduction electrons is possible. This could favor the helical or SDW states. In an RKKY mechanism, the spin periodicity should match that of the conduction electrons at the Fermi level. Our LDA band structure in Fig. 5 shows (k_x 0 0) crossings of the Fermi surface by spin up and down V 3d(t_{2g}) bands at $k_x = 0.15$ and 0.45, respectively. Neither matches the observed $k_x = 0.29$ spin modulation, although this does correspond to the difference between the two Fermi vectors. The present LDA results were obtained for a simple (0 0 0) ferromagnetic ordering of Mn moments, so a more self-consistent procedure is needed to evaluate whether the observed (0.29 0 0) magnetic vector matches a V 3d-band Fermi vector, because the V d-band structure is sensitive to the Mn exchange splitting and Mn-V spin coupling. Superexchange and RKKY couplings are not mutually exclusive—the Mn spin order in $MnVO_3$ may arise from cooperation or competition between the two interactions.

VII. CONCLUSIONS

$MnVO_3$ is an unusual perovskite, because the ground state is determined by interactions of localized *A*-site Mn^{2+} $3d^5$ and itinerant *B*-site V^{4+} $3d^1$ electrons. Alternative helical and SDW models for the observed (0.29 0 0) Mn magnetic order are both physically plausible, and the exchange interactions are likely to involve both Mn-O-Mn superexchange and RKKY coupling through the V d-band. Further experiments and calculations of the magnetic interactions are needed to elucidate the essential physics of the $MnVO_3$ ground state.

ACKNOWLEDGMENTS

We acknowledge the Engineering and Physical Sciences Research Council and Science and Technology Facilities Council for support and the provision of ESRF and ILL beam time, and the Leverhulme Trust for additional support.

*j.p.attfield@ed.ac.uk

[1] A. J. Williams, A. Gillies, J. P. Attfield, G. Heymann, H. Huppertz, M. J. Martínez-Lope, and J. A. Alonso, Phys. Rev. B **73**, 104409 (2006).

[2] J. S. Zhou, C. Q. Jin, Y. W. Long, L. X. Yang, and J. B. Goodenough, Phys. Rev. Lett. **96**, 046408 (2006)

[3] L. O. SanMartin, A. J. Williams, J. Rodgers, J. P. Attfield, G. Heymann, and H. Huppertz, Phys. Rev. Lett. **99**, 255701 (2007).

[4] S. A. J. Kimber, J. A. Rodgers, H. Wu, C. A. Murray, D. N. Argyriou, A. N. Fitch, D. I. Khomskii, and J. P. Attfield, Phys. Rev. Lett. **102**, 046409 (2009).

[5] J. G. Cheng, J. S. Zhou, and J. B. Goodenough, Phys. Rev. B **80**, 174426 (2009).

[6] I. A. Nekrasov, G. Keller, D. E. Kondakov, A. V. Kozhevnikov, Th. Pruschke, K. Held, D. Vollhardt, and V. I. Anisimov, Phys. Rev. B **72**, 155106 (2005).

[7] T. Yoshida, M. Hashimoto, T. Takizawa, A. Fujimori, M. Kubota, K. Ono, and H. Eisaki, Phys. Rev. B **82**, 085119 (2010).

[8] I. H. Inoue, C. Bergemann, I. Hase, and S. R. Julian, Phys. Rev. Lett. **88**, 236403 (2002).

[9] B. L. Chamberland and P. S. Danielson, J. Solid State Chem. **10**, 249 (1974).

[10] R. V. Shpanchenko, V. V. Chernaya, A. A. Tsirlin, P. S. Chizhov, D. E. Sklovsky, E. V. Antipov, E. P. Khlybov, V. Pomjakushin, A. M. Balagurov, J. E. Medvedeva, E. E. Kaul, and C. Geibel, Chem. Mater. **16**, 3267 (2004)

[11] A. A. Belik, M. Azuma, T. Saito, Y. Shimakawa, and M. Takano, Chem. Mater. **17**, 269 (2005).

[12] A. Kumar, L. W. Martin, S. Denev, J. B. Kortright, Y. Suzuki, R. Ramesh, and V. Gopalan, Phys. Rev. B **75**, 060101(R) (2007).

[13] A. Kumar, N. J. Podraza, S. Denev, J. Li, L. W. Martin, Y. Chu, R. Ramesh, R. W. Collins, and V. Gopalan, Appl. Phys. Lett. **92**, 231915 (2008)

[14] Y. Syono, S. Akimoto, and Y. Endoh, J. Phys. Chem. Solid. **32**, 243 (1971).

[15] J. Rodriguez-Carvajal, Phys. B **192**, 55 (1993).

[16] M. Kenzelmann, A. B. Harris, S. Jonas, C. Broholm, J. Schefer, S. B. Kim, C. L. Zhang, S. W. Cheong, O. P. Vajk, and J. W. Lynn, Phys. Rev. Lett. **95**, 087206 (2005).

[17] P. G. Radaelli and L. C. Chapon, Phys. Rev. B **76**, 054428 (2007).

[18] A. B. Harris, Phys. Rev. B **76**, 054447 (2007).

[19] P. Blaha, K. Schwarz, G. Madsen, D. Kvasnicka, and J. Luitz, WIEN2K code [http://www.wien2k.at].